electronics

MDPI

Article

A New Converter for a Switched Reluctance Generator

Guyuan Ji [1,*] and Kazuhiro Ohyama [2]

[1] School of Electrical Engineering, Shanghai Dianji University, Shanghai 201306, China
[2] Department of Electrical Engineering, Fukuoka Institute of Technology, Fukuoka 8110295, Japan
* Correspondence: jigy@sdju.edu.cn

Abstract

This paper proposes a type of converter suitable for switched reluctance generators (SRGs) with a new construction. The new topology of the converter does not require capacitors on the DC bus side and performs AC-AC conversion directly by controlling the generator through phase-to-phase voltage. It can reduce the capacitor charging structure, lower maintenance costs, reduce the impact of speed variations on interphase voltage, and enhance excitation. The paper will discuss in detail the working principle and characteristics of the proposed converter, and finally, it will verify the effectiveness of the proposed method based on the simulation results. Simulation results demonstrate the feasibility of the proposed topology for the generator application: the three-phase excitation currents reach a peak value of approximately 120 A, and the phase-to-phase voltage is maintained within the range of approximately 100 V under the simulated operating condition, with stable waveforms and no evident distortion, confirming that the proposed new converter can reliably drive the SRG.

Keywords: switched reluctance generator; capacitorless AC-AC converter; commutation method

1. Introduction

Against the background of increasingly urgent demands for energy efficiency and sustainable development and with growing global attention to environmental and energy issues, the demand for efficient, reliable, and environmentally friendly motor systems is constantly increasing. The Switched Reluctance Machine (SRM), a new type of machine, has attracted attention in the fields of electric vehicles, wind power generation, and aerospace in recent years owing to its unique structural advantages and high reliability, which enable it to operate in both motoring and generation mode [1–12]. Compared with permanent magnet synchronous motors (PMSMs) and induction motors (IMs), SRMs do not require permanent magnets. The rotor is composed solely of laminated iron cores, offering a simple structure, low manufacturing cost, and strong fault tolerance. In addition, an SRM can operate stably at high temperatures and variable speeds, with no risk of permanent magnets demagnetization. It shows great potential in extreme working conditions and has extensive application prospects.

At present, research on SRMs mainly focuses on optimizing the body structure, suppressing torque ripple, and controlling the maximum output power. In contrast, research on the topological structure of the converter in the primary circuit is relatively scarce. The topological structure and control strategy of the power converter for motors directly affect its system performance, torque ripple, noise, and energy conversion efficiency. Therefore,

Check for updates

Academic Editor: Dorin Petreus

Received: 24 July 2026
Revised: 7 September 2026
Accepted: 15 September 2026
Published: 19 September 2026

Copyright: © 2026 by the authors. Licensee MDPI, Basel, Switzerland. This article is an open access article distributed under the terms and conditions of the Creative Commons Attribution (CC BY) license.

research on converters for SRMs has become particularly important. With the popularization of SRM applications, research on the control of SRMs and on ensuring their smooth operation by exciting each phase winding of the motor through power converters has received attention [13–15]. Some studies have focused explicitly on the topology of DC-DC converters, which provide DC power. In [16], a DC-DC converter was proposed to eliminate the voltage imbalance problem in bipolar DC grids to supply power to multi-level switched reluctance motor drivers. Ref. [17] proposed a DC-DC converter that combines the Buck-Boost converter with the Sepic converter and is applied to the SRM power pumping system, which can minimize switching and maintain the balance of the two input capacitors. Moreover, some research has focused on DC-DC converters for specific applications. For example, in the self-powered agricultural pump system [18], a novel central-switching DC-DC converter is adopted to optimize the output power of the self-assisted photovoltaic (PV) array without using any input PV capacitors, which minimizes switching losses and improves the overall system efficiency. In addition, there is some research on DC-AC converters for driving SRMs. In reference [19], a six-switch inverter specifically for commercial use was proposed, which can minimize overall system size and cost while improving efficiency. In [20–22], new types of converters are proposed by increasing or decreasing the number of switches used based on the phase number of the motor, which overcomes the limitation of the power supply configuration, improves the utilization rate of the equipment, and achieves low cost and high efficiency. Moreover, some studies have used the multilevel principle to research new DC-AC converter topologies. Refs. [23–26] proposed a new multilevel converter topology for SRM drivers with transistor fault tolerance capability to avoid the use of additional transistors, excessive quantities, and static or mechanical relays. Other research has focused on DC-AC converter designs tailored for specific applications. For example, in the wind power system [27], to address the problem of low output power at low speed when the SRM operates in the power-generation state, a new power converter topology is proposed to improve the performance of traditional power converters.

According to relevant research, SRM converters typically use asymmetric half-bridge converters [28–30], which require a two-stage conversion process from AC to DC, followed by DC to AC. In this conversion, large-volume DC-link capacitors are used to smooth the rectified AC voltage. These capacitors not only increase the system volume but also introduce reliability issues due to their tendency to fail easily. At the same time, long-term operation will also affect the lifespan of the electrolytic capacitors used in the DC-link and increase maintenance costs. However, in current research on new topologies, improvements still need to be made on the basis of the DC link. There are no examples of converters that omit the intermediate DC-link in SRM applications. This paper proposes a direct AC-AC converter without a DC bus capacitor, which is suitable for a switched reluctance generator (SRG). This converter, through a matrix topology, directly converts the alternating-current (AC) electrical energy into the AC power required by the generator, thereby eliminating the two-stage power conversion (rectification and inversion) and the large-capacity DC-link capacitors used in traditional schemes. The system structure is simplified, and reliability is enhanced. The effectiveness of the proposed converter was verified through Matlab/Simulink2023b [31–35].

The remainder of this paper is organized as follows. Section 2 introduces the AC-AC converter. Section 3 describes the methodology Section 4 presents the simulation results. Section 5 presents a discussion, and Section 6 concludes the paper.

2. New AC-AC Converter

2.1. Structure of the Converter

The capacitorless AC-AC converter for SRG proposed in this paper has an array structure and consists of 36 switches. Figure 1 illustrates the circuit topology of the converter. This topology enables the converter to be connected to each independent winding of the SRG. The 36 switches are composed of 18 bidirectional switches, each bidirectional switch containing two IGBTs and two diodes. The power switches used in the proposed topology are selected as IGBT modules, with a forward voltage of 1 V and an initial current of 0 A. The diodes feature a forward voltage of 0.8 V. On the input side, the converter is connected to three-phase AC power supplies labeled V_r, V_s, and V_t, and the output side is connected to each phase winding of the SRG.

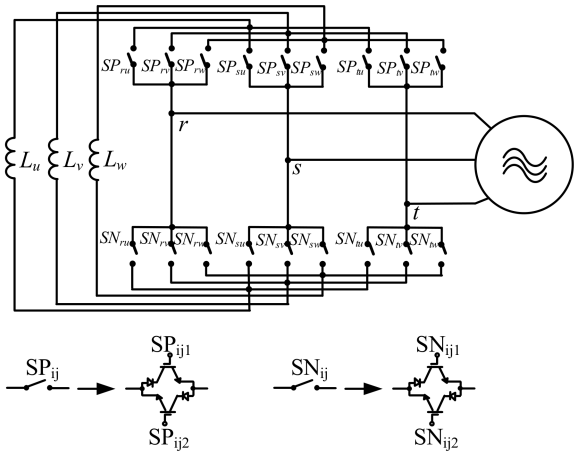


Figure 1. Circuit topology of AC–AC converter.

Since each phase winding of the SRG is independent, each switch in the capacitorless AC-AC converter is designated as SP_{ij} $(i = r, s, t; j = u, v, w)$, where SP_{ij} denotes the switch connected to the positive terminal of the excitation winding, while the switch connected to the negative terminal is labeled SN_{ij} $(i = r, s, t; j = u, v, w)$.

According to the structure of the capacitorless AC-AC converter shown in Figure 1, the voltage applied to each winding of the SRG is determined by the conduction state of the converter switch. Specifically, the voltage V_j $(j = u, v, w)$ across any phase winding L_j (j = u, v, w) applied to the SRG is jointly determined by the phase voltage (V_r, V_s, V_t) of the three-phase AC power supply and the conduction switches SP_{ij}/SN_{ij} $(i = r, s, t; j = u, v, w)$. Here, the phase voltage (V_r, V_s, V_t) and interphase voltage (V_{rs}, V_{st}, V_{tr}) on the three-phase AC power supply side are expressed by Equations (1)–(3) according to the phase voltage amplitude E and the power supply frequency ω [36,37]. Equation (1) gives the three input phase voltages, which constitute a symmetric three-phase set mutually shifted by 120° in electrical angle. Using the trigonometric identity, the amplitude of any line-to-line voltage is $\sqrt{3}$ times the phase-voltage amplitude and leads the corresponding phase voltage by 30°. This relationship is an intrinsic property of the three-phase system.

$$\begin{bmatrix} V_r \\ V_s \\ V_t \end{bmatrix} = E \begin{bmatrix} \cos\theta \\ \cos(\theta - 2\pi/3) \\ \cos(\theta + 2\pi/3) \end{bmatrix} \tag{1}$$

$$\begin{bmatrix} V_{rs} \\ V_{st} \\ V_{tr} \end{bmatrix} = \begin{bmatrix} V_r - V_s \\ V_s - V_t \\ V_t - V_r \end{bmatrix} = \sqrt{3}E \begin{bmatrix} \cos(\theta + \pi/6) \\ \cos(\theta - \pi/2) \\ \cos(\theta + 5\pi/6) \end{bmatrix} \tag{2}$$

$$\theta = \omega t, \tag{3}$$

By controlling the individual switches of the capacitorless AC-AC converter, the phase voltages from the power supply side are converted into excitation voltages for the generator according to the switch states and are applied to each phase winding of the SRG. At this time, the states of the switches in the capacitorless AC-AC converter can thus be represented by a matrix denoted as T. This matrix is defined by Equations (4) and (5), which describe the conduction state of the switches (SP_{ij}/SN_{ij}) in the converter. The transformation matrix T in Equation (4) is composed of two rows. The first row gathers the positive-switch states and acts as a spatial selection vector that maps the three input phase voltages onto the output terminal through the upper switches. The second row gathers (with a negative sign) the negative-switch states. Consequently, each column of T corresponds to one input phase, and the matrix multiplication in Equation (6) implements a linear combination of the input phase voltages weighted by the switch states. The voltage V_j (j = u, v, w) applied to each excitation winding is expressed by the product Equation (6) of the matrix T and the phase voltage (V_r, V_s, V_t) [38–41].

$$T = \begin{bmatrix} SP_{rj} & SP_{sj} & SP_{tj} \\ -SN_{rj} & -SN_{sj} & -SN_{tj} \end{bmatrix} \tag{4}$$

$$SP_{ij}/SN_{ij} = \begin{cases} 1 & on \\ 0 & off \end{cases} (i = r, s, t;\ j = u, v, w) \tag{5}$$

$$V_j = \begin{bmatrix} SP_{rj} & SP_{sj} & SP_{tj} \\ -SN_{rj} & -SN_{sj} & -SN_{tj} \end{bmatrix} \begin{bmatrix} V_r \\ V_s \\ V_t \end{bmatrix} \tag{6}$$

2.2. Commutation Mode of the Converter

Based on the Equations (1)–(6), it is emphasized that the switching states are not arbitrary and must satisfy two fundamental constraints to ensure safe operation of the matrix converter: 1. no input short circuit; 2. no output open-circuit.

The topological structure of a single-phase capacitorless AC-AC converter is shown in Figure 2. In the figure, the addition of characters “N” and “P” on the U-phase winding represents the direction of the current. Here, “N” indicates the current flowing from the positive terminal to the negative terminal in the SRM winding, while “P” indicates the current flowing in the opposite direction. When the converter is in operation, both the top and bottom of the bidirectional switch are conducting, and the winding current can be bidirectionally energized for commutation. Therefore, to prevent current paths from being cut off and power supply short circuits during commutation, it is necessary to ensure that the current path remains intact.

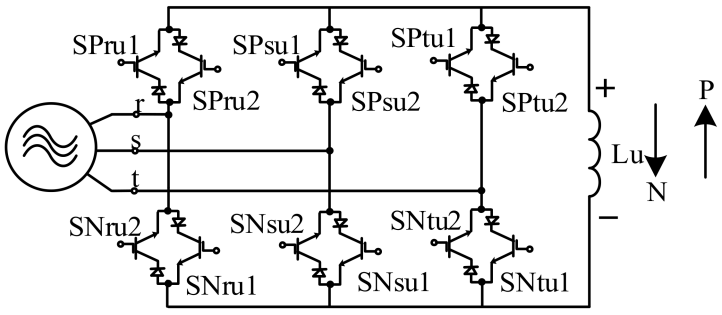


Figure 2. Circuit topology of U-phase.

2.2.1. Preventing the Interruption of Current Path

Figure 3a shows a state in which the current path is interrupted. For example, when commutation is initiated from phase r to another phase while the current is flowing in the N direction (from the positive terminal to the negative terminal), switch SP_{ru1} is turned on, while current is still flowing, but all other switches remain off. The current path is cut off, making commutation impossible. Therefore, during converter operation, it is essential to prevent two scenarios: the interruption of the current path between switches on the same terminal side and interruption between switches on opposite terminal sides.

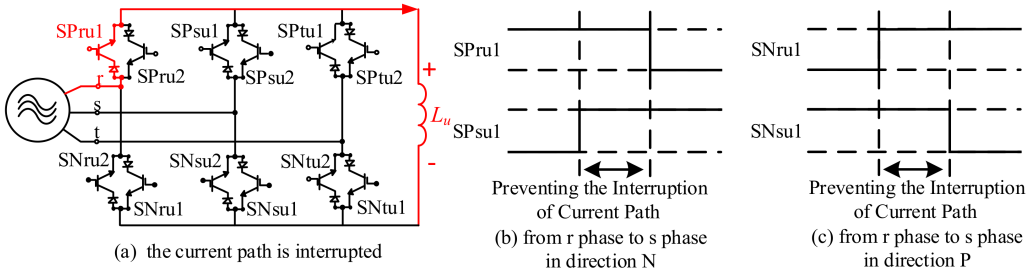


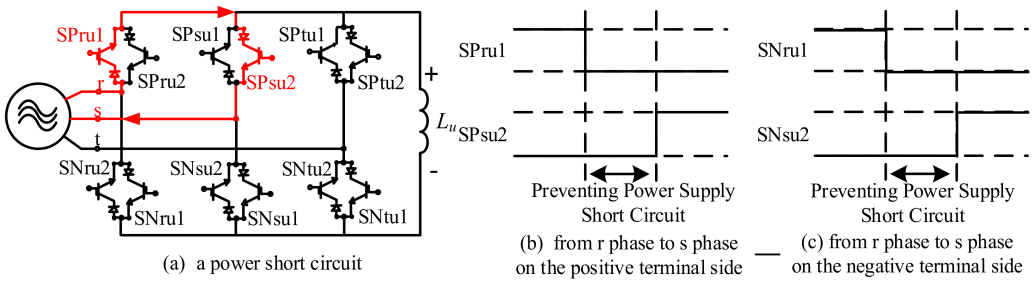
Figure 3. State of current path interruption.

Figure 3b,c show a commutation method that prevents current interruption on the same terminal side. Figure 3b shows the commutation process from r phase to s phase while the current is flowing in direction N. To ensure a continuous current path when switch SP_{ru1} is turning off, switch SP_{su1} must be turned on before switch SP_{ru1} is turned off, thereby maintaining current continuity. Figure 3c depicts the commutation from r phase to s phase when the current is initially flowing in direction P. To prevent the current path from being interrupted, switch SN_{ru1} should be turned on before switch SN_{su1} is turned off. Furthermore, preventing the interruption of the current path in the P direction (from the negative side to the positive terminal) is the same as that described.

2.2.2. Preventing the Power Short Circuit

Figure 4a shows the state of a power short circuit when the current flows in the direction N (from the positive terminal to the negative terminal) during commutation from phase r to phase s, as shown in the figure. When the voltage of r phase is higher than that of s phase, the switches SP_{ru1} and SP_{su2} are simultaneously turned on, and a large current will flow from switch SP_{ru1} to SP_{su2}, resulting in a power supply short circuit. To prevent a power short circuit, the bidirectional switch should be controlled in the commutation mode shown in Figure 4b,c. Figure 4b shows the commutation mode of switch SP_{ru1} and switch SP_{su2} on the positive terminal side of the coil when commutating from r phase to s phase to prevent a power short circuit. When SP_{ru1} is turned off and SP_{su2} is not connected to the power supply, the power short circuit caused by the on-off switching of the two switches is prevented by keeping the two switches disconnected for a certain period of time. Figure 4c shows the commutation mode of switch SN_{ru1} and switch SN_{su2} on the negative terminal side of the coil when commutating from r phase to s phase to prevent power short circuit. When SN_{ru1} and SN_{su2} are turned off at the same time, no power short circuit will occur.

Therefore, in the capacitorless AC-AC converter, there are nine switching modes for each phase as shown in Table 1. In addition, the capacitorless AC-AC converter uses a four-step commutation method. The method is based on detecting the magnitude relationship between the phase-to-phase voltages and the polarity of the phase current. The commutation is carried out through four steps to avoid power short circuit and current path interruptions.



(a) a power short circuit (b) from r phase to s phase on the positive terminal side (c) from r phase to s phase on the negative terminal side

Figure 4. The state of a power short circuit.

Table 1. Switching mode.

Switching Mode	U Phase						
	SPru	SPsu	SPtu	SNru	SNsu	SNtu	Vu
1	1	0	0	1	0	0	0
2	1	0	0	0	1	0	Vrs
3	1	0	0	0	0	1	Vrt
4	0	1	0	1	0	0	Vsr
5	0	1	0	0	1	0	0
6	0	1	0	0	0	1	Vst
7	0	0	1	1	0	0	Vtr
8	0	0	1	0	1	0	Vts
9	0	0	1	0	0	1	0

3. Control Method

3.1. Overview of Control Method

The proposed control method for capacitorless AC-AC converters suitable for SRG can be divided into five operating states: pre-excitation state, excitation state, transition from excitation to power-generation state, power-generation state, and after-power-generation state. In the pre-excitation state, the maximum phase voltage for the SRG is selected from the starting angle to the turn-on angle, which is the rotor position angle that determines when the winding begins to be energized for excitation. During this state, the excitation voltage of the winding is zero because the potentials between the positive and negative terminals of the winding are equal. Then, during the excitation state, the maximum phase-to-phase voltage is selected from the turn-on angle to the turn-off angle, which is the rotor position angle that controls the end of winding excitation and the switch to the power generation feedback state. In this state, the potential between the positive and negative terminals of the winding is the difference value between the high and low potentials, resulting in the excitation voltage of the winding being the difference between the maximum and minimum phase voltages. When transitioning to the power-generation state at the turn-off angle, the maximum phase-to-phase voltage is changed to the minimum phase-to-phase voltage for the corresponding commutation. During the power-generation state, the minimum phase-to-phase voltage is selected from the turn-off angle to the regeneration end angle (energy recovery state). During this selection, the potential between the positive and negative terminals of the winding is the negative difference value between the minimum and maximum potentials, meaning the induced voltage of the winding is the difference between the minimum and maximum phase voltages. After the power-generation state, the final state occurs from the regeneration end angle to the stop angle, where the minimum phase voltage is selected. In this condition, the excitation voltage of the winding is zero as the potential between the positive and negative terminals of the winding is again equal, completing the entire commutation process during SRG operation.

In this article, the 12/8 pole SRG was selected as shown in Table 2, which is one of the most commonly used three-phase switched reluctance structures, offering a good trade-off between torque ripple suppression and structural complexity [42]. The 12/8 pole SRG configuration enables dual-channel operation and can switch to a single-channel fault-tolerant mode in the event of a channel failure, thereby improving the reliability of the power supply system an important requirement for wind power generation [43]. For the 12/8 pole SRG, each time a new phase is excited, the equilibrium position of the rotor advances by 15°, so after one complete cycle, the angle turned through is 45°. In this way, the conduction intervals of the three phases and their spatial phase relationships determine the commutation sequence within each rotor pole pitch. For example, as shown in Figure 5, when the turn-on and turn-off angles are set to the values shown according to the rotor position, the commutation method proposed above is described. The turn-on angle θ_{on} and turn-off angle θ_{off} are determined beforehand according to the given generator operating point (rotor speed and load torque) by ordinary least squares.

Table 2. Parameters.

Rated output	3.5 kW
Number of coil turns	44
Stator pole	12
Rotor pole	8
Resistance	0.053
Flux linkage	0.0035

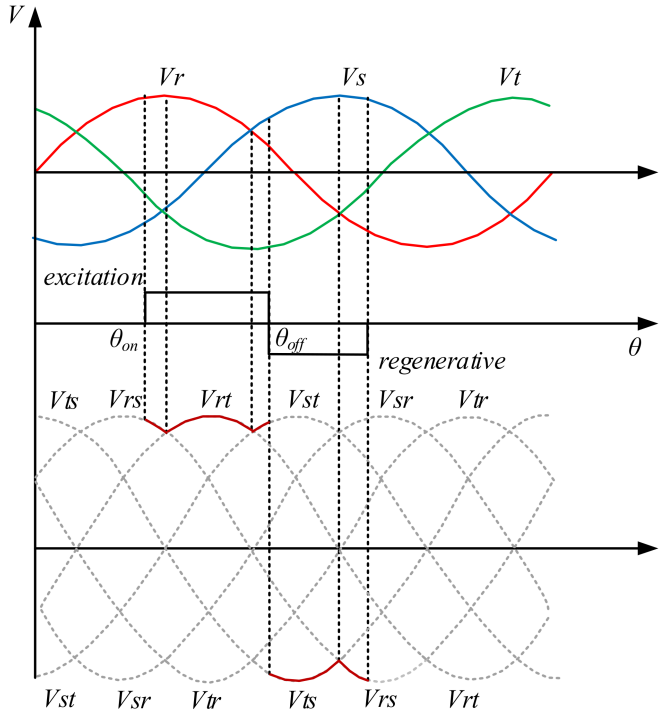


Figure 5. Excitation using 3 phase voltage.

As shown in Figure 5, when going from the starting angle (0°) to the turn-on angle (θ_{on}), the maximum phase voltage V_{tt} is selected at the starting state before the electric operation. During this period, the maximum phase-to-phase voltage from V_{tt} to V_{rr} continues to excite due to the three-phase voltage change. When the turn-on angle reaches the turn-off angle (the period from θ_{on} to θ_{off}), the maximum phase-to-phase voltage is

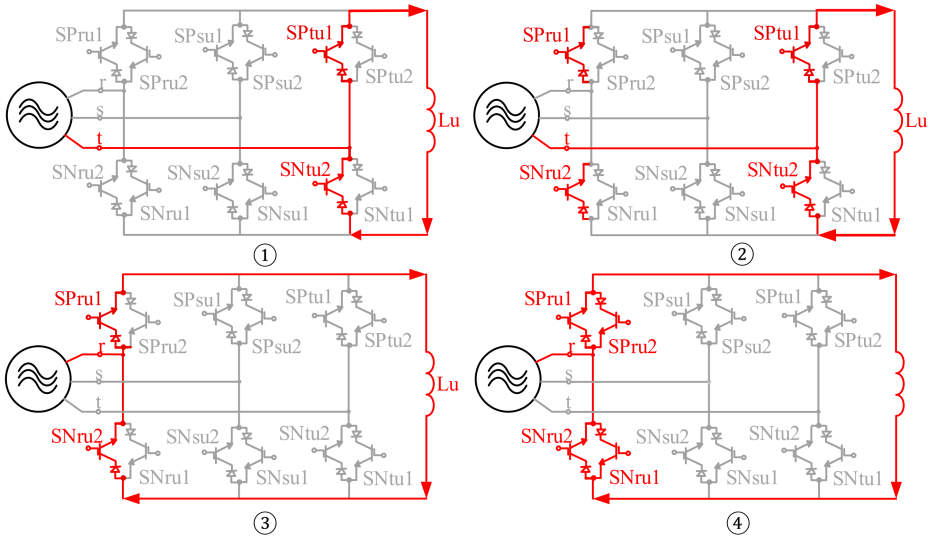
continuously V_{rs}, marking the start of the excitation state. During the excitation state, the excitation current builds up rapidly. At this time, the maximum phase-to-phase voltage switches from V_{rt} to V_{st}, and the SRG continues to operate in the electric operation state. When θ is at the position of θ_{off}, the SRG from the electric operation state changes to the power-generation operation state, and the phase-to-phase voltage switches from V_{st} to Vts. During operation, the minimum phase-to-phase voltage change V_{ts} to V_{rs} (from end angle θ_{off} to regeneration end angle) occurs in the continuous power-generation operation mode. Finally, from the regeneration end angle to the stop angle (45°), the minimum phase-to-phase voltage V_{rr} is selected to conclude the entire commutation operation.

3.2. Commutation Method

For the SRG, the energy from the three-phase AC power is supplied to the winding through a capacitorless AC-AC converter. Therefore, the control method of this converter directly affects the operation of the SRG. A control method suitable for the SRG was proposed based on the design of the capacitorless AC-AC converter. When the SRG is operating, the maximum phase-to-phase voltage is utilized in the excitation state, while the minimum phase-to-phase voltage is selected during the power-generation state. The 4-step commutation method was employed to switch the voltage between the selected two phases. Figure 6 shows the four-step commutation process of a 12/8 SRG within one electrical cycle based on the Figure 5, which included (a) pre-excitation state, (b) excitation state, (c) transition from excitation to generating mode, and (d) generating state. The red path with arrow in Figure 6 represents the current-flowing route via the conducting switches.

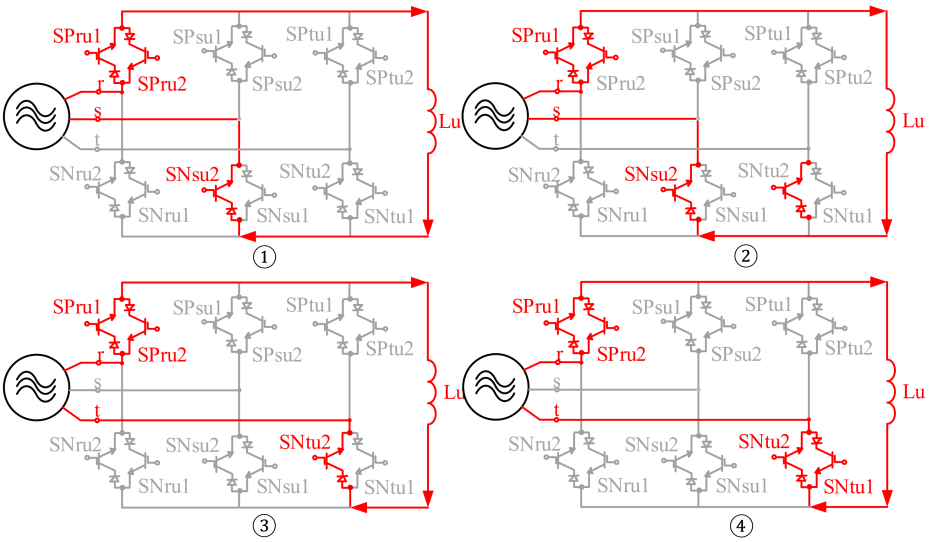
- Pre-excitation state.

As shown in Figure 6a, the commutation method was employed when the maximum phase-to-phase voltage transitions from V_{tt} to V_{rr}. In order to prevent excessive power generation, SP_{ru1} and SP_{tu2} were kept continuously turned on. Before the electric operation state, since the potentials at the positive and negative terminals of the winding were equal, the excitation voltage across the winding wass zero at that time.

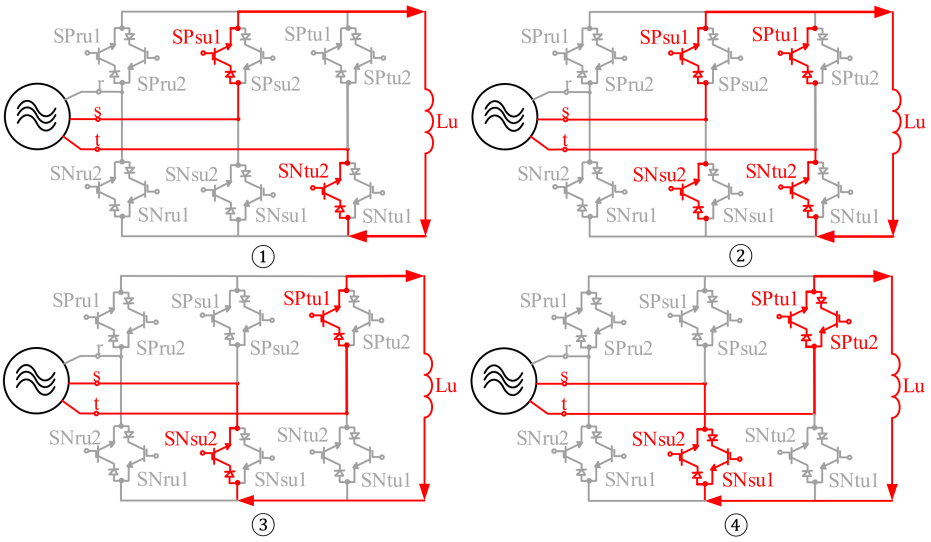


(**a**) Pre-excitation state.

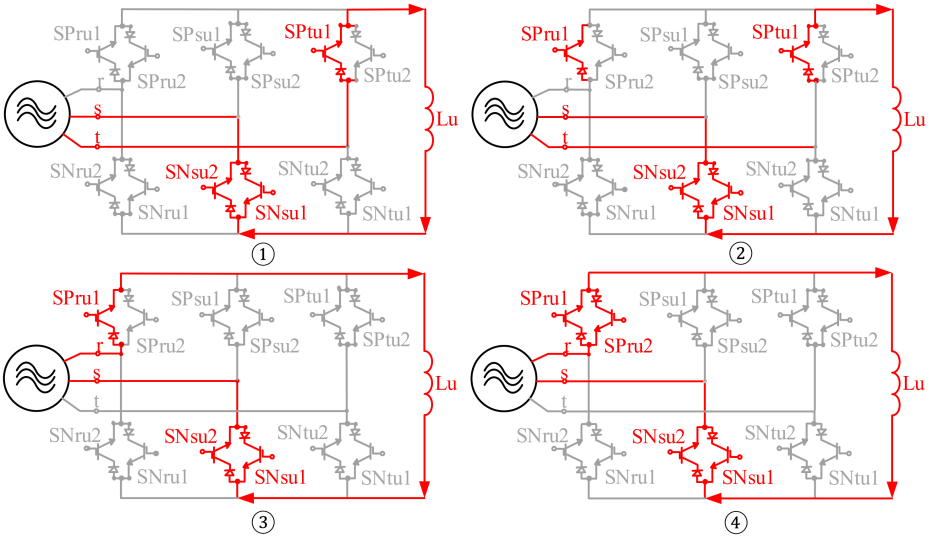
Figure 6. *Cont.*



(**b**) Excitation state.



(**c**) Transition from excitation to power-generation state.



(**d**) Power-generation state.

Figure 6. Commutation method for change phase.

- Excitation state.

As shown in Figure 6b, following the SRG operation, the commutation method changed the applied phase-to-phase voltage from V_{rs} to V_{rt}, keeping the U-phase current Iu flowing in the positive direction. During the excitation state, the process began as follows: Firstly, at step 1, the switch SN_{su1} was turned off. At this time, the current Iu flowed to SN_{su2}, and the switch SN_{su1} that was turning off had no effect on the circuit. Then, at step 2, switch SN_{tu2} was turned on. At this time, since $V_s < V_t$, the current continued to flow from SP_{ru1} to SN_{su2}. Next, in step 3, V_s became greater than V_t. The current stopped flowing to the switch SN_{su2} that was turned off. The current path now shifted from SP_{ru1} to SN_{tu2}. Finally, the switch SN_{tu1} was turned on at Step 4, and the commutation from the rs phase to the rt phase was completed.

- Transition from excitation to power-generation state.

As shown in Figure 6c, the commutation method was employed when the applied phase-to-phase voltage was switched from V_{st} to V_{ts} while keeping the U-phase current Iu flowing in the positive direction. This transition occurred from the excitation state to the generation state. Firstly, in step 1, switch SP_{su1} and SN_{tu2} were turned on, allowing the current Iu flows from SP_{su1} to SN_{tu2}. In step 2, the switch SP_{tu1} and SN_{su2} were turned on. Since $V_s < V_t$, the current continued to flow from SP_{su1} to SN_{tu2}. Next, in step 3, there was a change where V_t became greater than Vs. At this point, the current stopped flowing to the switch SP_{su1} and SN_{tu2}, and the switches were turned off. The current path switched from Sptu1 to SN_{su2}. Finally, in the step 4, the switches SP_{tu1} and SN_{su1} were turned on, completing the commutation from the st phase to the phase.

- Power-generation state.

As shown in Figure 6d, in the generation operation state, the commutation method was used when the applied phase-to-phase voltage was switched from V_{ts} to V_{rs} while maintaining the U-phase current Iu flowing in the positive direction. Firstly, at step 1 switch SP_{tu2} was turned off. At this time, the current Iu flowed from SP_{tu1} to SN_{su2}. Then, at step 2, switch SP_{ru1} was turned on. At this time, since $V_r < V_t$, the current continued to flow from SP_{tu1} to SN_{su2}. Next, in step 3, the SP_{tu1} was turned off. The current path switched from switch SP_{ru1} to SN_{tu2}. Finally, SP_{ru2} was turned on at Step 4, and the commutation from the ts phase to the rs phase was completed.

- After-power-generation state.

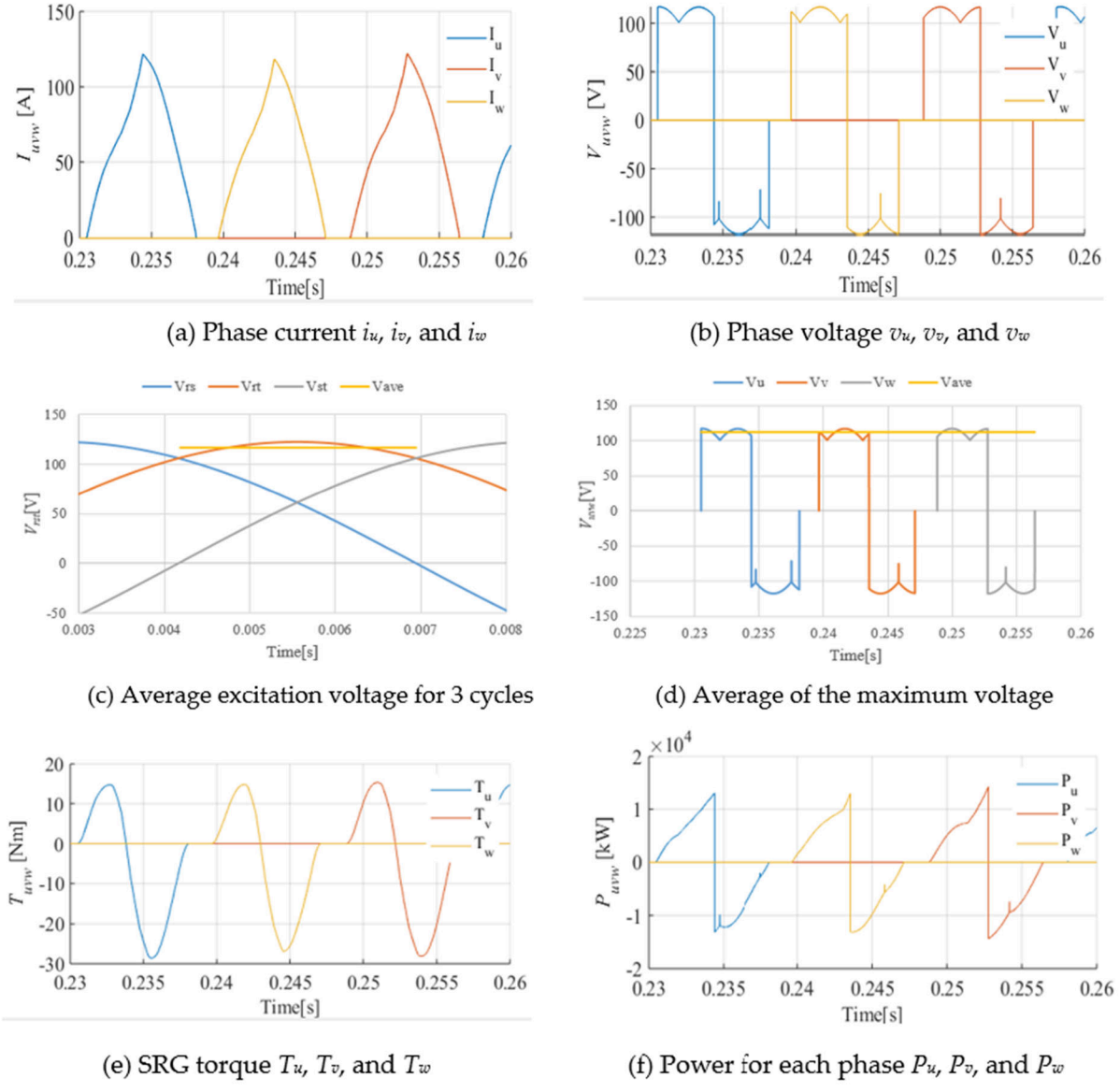
In addition, since the commutation method before activation is the same as that after regeneration, in the case of commutation after regeneration, the corresponding switch can be directly applied for commutation.

4. Results

Based on the proposed capacitorless AC-AC converter and commutation mode for SRG, the simulation results were verified using MATLAB/Simulink. Figure 7 shows the transient response of SRG using new converter under 120 V, 60 Hz three-phase voltage power.

As shown in Figure 7a, the phase currents Iu, Iv, and Iw exhibited a pulse shape that first rises and then falls. The rising section is the excitation period, and the falling section is the power generation feedback period. This ensures that it operates in a power-generation state. Based on the provided torque and power waveform diagrams, the operating state of the SRG can be summarized that the electromagnetic torque of each phase varies periodically and exhibits negative torque (braking torque) during the generating stage, opposing the rotor's direction of rotation, which aligns with the characteristics

of generating operation. The instantaneous power of each phase shows positive pulse outputs during the generating intervals, indicating that energy is being fed back from the mechanical side to the electrical side. The torque and power waveforms correspond consistently in timing, with peaks occurring in the region of the maximum rate of change of inductance, verifying the rationality of the control angle settings. Additionally, the periodicity and symmetry of the waveforms reflect the stable generating operation of the motor under four-step commutation method. As shown in Figure 7b, with the phase voltages Vu, Vv, and Vw, it can be obtained that this waveform satisfies the proposed control method of the generator based on the rotor position using the phase-to-phase voltage.



(a) Phase current i_u, i_v, and i_w

(b) Phase voltage v_u, v_v, and v_w

(c) Average excitation voltage for 3 cycles

(d) Average of the maximum voltage

(e) SRG torque T_u, T_v, and T_w

(f) Power for each phase P_u, P_v, and P_w

Figure 7. Transient response of SRG using new converter.

As shown in the Figure 7c, the voltage of each phase is the sharp of the phase-to-phase voltage, which is different with the DC voltage applied to SRG in general, as it is constantly changing over time. The influence of the time variation in the phase-to-phase voltage is averaged by the excitation, which is repeated over a short period of time. Compared with the average value of the maximum three-phase voltage 116.96 V, the average phase voltage of the three periods shown in this figure shown in Figure 7d is 113.5 V. It can be seen from

the electricity that the influence of the time variation of the phase-to-phase voltage is very small, and the generated torque Tu, Tv, Tw and power Pu, Pv, Pw were in Figure 7e,f.

5. Discussion

The simulation results presented in Section 4 confirm the feasibility of the proposed converter topology for the switched reluctance generator (SRG) application, demonstrating that balanced three-phase excitation currents and stable phase-to-phase voltages can be maintained during steady-state operation. Nevertheless, several aspects deserve further discussion.

(1) In the existing literature, the asymmetric half-bridge inverter combined with a PWM rectifier is the most widely adopted configuration for switched reluctance drive/generator systems, as it provides independent control over each phase and inherently supports the freewheeling of phase currents. However, this conventional topology relies on a bulky DC-bus capacitor and a separate rectification stage. The proposed converter, by removing the DC-bus capacitor and performing AC-AC conversion directly through phase-to-phase voltage control, reduces the capacitor charging structure and lowers maintenance costs. This trade-off between structural simplicity and control complexity is worth emphasizing: while the proposed topology eliminates the DC-link capacitor, it places additional requirements on the phase-to-phase voltage control strategy to ensure balanced excitation.

(2) A fundamental consequence of removing the DC-link capacitor is the increase in the number of active switching devices, and the associated trade off must be evaluated from several perspectives. (1) Switching loss: Because the converter operates through phase-to-phase voltage control with more frequent switching actions, the total switching loss may be higher than that of the conventional topology at comparable operating points, although the reduced passive components lower the associated losses. (2) Reliability: On the one hand, eliminating the electrolytic DC-link capacitor removes a well-known failure prone and thermally stressed component, improving long-term reliability; on the other hand, the higher switch count introduces additional semiconductor failure points, so the net reliability depends on the balance between these two effects. (3) Cost: The savings from removing the bulky capacitor and the rectification stage may be partially offset by the cost of additional switches and associated circuitry; a quantitative cost comparison is therefore needed for practical deployment.

(3) Quantitative performance indicators such as efficiency, torque ripple, current ripple, output power, and voltage utilization have not yet been systematically evaluated in the present work. Furthermore, the dynamic response under load transients, parameter variations, and grid-connected conditions requires further investigation. These constitute the main limitations of the present study.

(4) The current study is based on simulation validation and focuses primarily on demonstrating the feasibility of the proposed topology. Beyond the simulation results reported here, the practical feasibility of the proposed capacitorless converter must ultimately be verified on a laboratory prototype. The commutation scheduling, the dead-time setting, and the phase-to-phase voltage balancing control should be validated under real device-switching behavior, on-state voltage drops, and parasitic parameters, none of which can be fully represented in an ideal simulation. As an intermediate step, hardware-in-the-loop (HIL) verification is planned to test the switching logic and the control algorithm in real time before physical implementation. The experimental evaluation will provide convincing evidence of the converter's performance beyond the simulated operating points.

(5) In this paper, the original work focuses on the topology, commutation, and control of the capacitorless converter itself, and it does not explicitly target any specific application scenario. Given the elimination of the DC-link capacitor, the proposed converter features reduced passive components, lower system volume, and weight attributes that are particularly attractive to application such as wind power generation systems, high-speed flywheel energy storage and aerospace starter/generator units. In these extensions, the increased switching loss and the higher control complexity inherent in the capacitorless design must be carefully weighed, and the control strategies will need to be adapted to the specific speed, power, and ambient-temperature ranges of each application.

6. Conclusions

In this paper, a capacitorless AC-AC converter was proposed for the 12/8 SRG and was established in Matlab/Simulink. The proposed capacitorless AC-AC converter has no DC link part to provide a possibility for the realization of low maintenance cost and high performance. The commutation method is explained, and the performance of the proposed new converter is examined. From the simulation results, it is verified that the capacitorless AC-AC converter can successfully drive the SRG, and the validity of the commutation method is fully verified.

In the future, the proposed method and the traditional method (asymmetric half-bridge inverter + PWM converter) will be tested to compare the power loss and efficiency of each component, such as an SRG and converter. We also plan to compare and examine the impact on commercial power supplies when connected to the grid. A systematic evaluation over multiple rotor speeds, load conditions, excitation levels, and phase-voltage disturbances, together with quantitative performance indicators (efficiency, torque ripple, current ripple, output power, and voltage utilization), is an important part of our ongoing work and will be presented in detail in a follow-up paper.

Author Contributions: Conceptualization, G.J. and K.O.; methodology, G.J. and K.O.; validation, G.J.; investigation, G.J. and K.O.; resources, K.O.; data curation, G.J.; writing—original draft preparation, G.J.; writing—review and editing, G.J. and K.O.; supervision, K.O. All authors have read and agreed to the published version of the manuscript.

Funding: This research received no external funding.

Data Availability Statement: The data presented in this study are available on request from the corresponding author.

Conflicts of Interest: The authors declare no conflicts of interest.

References

1. Kakinuma, R.; Yamamura, N.; Ishida, M. Analysis of Maximum Power Point Mechanism of Small Wind Power Generation System Using SRG. In Proceedings of the 2021 24th International Conference on Electrical Machines and Systems (ICEMS), Gyeongju, Republic of Korea, 31 October–3 November 2021; pp. 762–765.
2. Bouklata, A.; Oubouaddi, H.; Brouri, A.; Mosaad, M.I.; Giri, F. Advanced Control Strategy of Switched Reluctance Generator-Based Wind Energy Conversion Systems Using Backstepping and Extremum Seeking Techniques. *IFAC-PapersOnLine* **2024**, *58*, 593–598. [CrossRef]
3. Touati, Z.; Moretti, G.; Khedher, A.; Zaccarian, L. Control and maximum power extraction of a switched reluctance generator with low resolution pulse-based position estimation. *J. Frankl. Inst.* **2025**, *362*, 107757. [CrossRef]
4. Zhi, X.; Duan, X.J.; Liu, L. MPPT for wind power system with switched reluctance generator. In Proceedings of the 2018 13th IEEE Conference on Industrial Electronics and Applications (ICIEA), Wuhan, China, 31 May–2 June 2018; pp. 1420–1424.
5. Mapa, S.; Maheswari, R.; Bhuvaneswari, G. Maximum Power Point Tracking Using a Novel Current Control Strategy in an SRG Based Variable Speed Wind Energy Conversion System. In Proceedings of the 2018 8th IEEE India International Conference on Power Electronics (IICPE), Jaipur, India, 13–15 December 2018.

6. Boumaalif, Y.; Ouadi, H.; Giri, H. Multi-stage adaptive speed control with torque ripple optimization for a switched reluctance motor in electric vehicle applications. *Engineering* **2025**, *58*, 104245.
7. Sreeram, K.; Jacob, C.M.; Cyril, M.; Punnen, A.R.; James, J. Optimization of Switched Reluctance Motor (SRM) Drive for Torque Ripple Mitigation and Cost Reduction in Plug-in Hybrid Electric Vehicle (PHEV). In Proceedings of the 2025 IEEE International Transportation Electrification Conference (ITEC-India), Pune, India, 16–19 September 2025.
8. Kumar, A.; Singh, B. DTC Based Solar fed SRM Drive for Electric Vehicle with Regenerative Braking Employing Zeta Converter. In Proceedings of the 2021 IEEE 6th International Conference on Computing, Communication and Automation (ICCCA), Arad, Romania, 17–19 December 2021; pp. 100–105.
9. Ajie, I.K.; Furqani, I.; Fadillah, A. Optimization of Switched Reluctance Motor for Two Wheels Electric Vehicle. In Proceedings of the 2023 International Conference on Electrical Engineering and Informatics (ICEEI), Bandung, Indonesia, 10–11 October 2023.
10. Deepak, M.; Janaki, G.; Bharatiraja, C. Optimize SRM Rotor Geometry Analysis for 3kW Light Electric Vehicle Grade Performances. In Proceedings of the 2022 International Interdisciplinary Conference on Mathematics, Engineering and Science (MESIICON), Durgapur, India, 11–12 November 2022.
11. Krishnan, R.; Blanding, D.; Bhanot, A.; Staley, A.; Lobo, N. High Reliability SRM Drive System for Aerospace Applications. In Proceedings of the IECON'03. 29th Annual Conference of the IEEE Industrial Electronics Society (IEEE Cat. No.03CH37468), Roanoke, VA, USA, 2–6 November 2003; pp. 1110–1115.
12. Ullah, S.; McDonald, S.P.; Martin, R.; Benarous, M.; Atkinson, G.J. A Permanent Magnet Assist, Segmented Rotor, Switched Reluctance Drive for Fault Tolerant Aerospace Applications. *IEEE Trans. Ind. Appl.* **2019**, *55*, 298–305. [CrossRef]
13. Khan, Y.A.; Twinkle, I.; Kumar, S.; Verma, V. Comparative Analysis of Different Converter Topologies for an SRM Drive with Conventional and Vector Control Schemes. In Proceedings of the 2020 International Conference on Emerging Frontiers in Electrical and Electronic Technologies (ICEFEET), Patna, India, 10–11 July 2020.
14. Zhu, Y.; Mao, Y.; Liu, P.; Liu, C.; Qian, Y.; Zhu, X. Comparison and analysis of two power topologies for four-phase SRM. In Proceedings of the 2021 IEEE 4th Student Conference on Electric Machines and Systems (SCEMS), Huzhou, China, 1–3 December 2021.
15. Pittermann, M.; Fort, J.; Diesl, J.; Pavlicek, V. Converters for Switched Reluctance Motor–Topology Comparison. In Proceedings of the 2018 18th International Conference on Mechatronics–Mechatronika (ME), Brno, Czech Republic, 5–7 December 2018.
16. Pires, V.F.; Foito, D.; Pires, A.J.; Cordeiro, A.; Martins, J.F. A DC-DC Converter for Bipolar DC Microgrids with Voltage Balance Capability to Supply a Multilevel SRM Drive. In Proceedings of the 2021 IEEE 15th International Conference on Compatibility, Power Electronics and Power Engineering (CPE-POWERENG), Florence, Italy, 14–16 July 2021.
17. Foito, D.; Pires, V.F.; Cordeiro, A.; Amaral, T.G.; Chaves, M.; Pires, A.; Martins, J.F. A SRM for a PV Powered Water Pumping System Based on a Multilevel Converter and DC/DC Dual Output Converter. In Proceedings of the 2022 7th International Conference on Smart and Sustainable Technologies (SpliTech), Split/Bol, Croatia, 5–8 July 2022.
18. Mishra, A.K.; Singh, B. Design of Autonomous Solar Powered SRM Based Agriculture Pump Utilizing Novel Central Switch DC-DC Converter. In Proceedings of the 4th IEEE Uttar Pradesh Section International Conference on Electrical, Computer and Electronics (UPCON), Mathura, India, 26–28 October 2017; pp. 549–555.
19. Kim, Y.C.; Yoon, Y.H.; Lee, B.K. A New Cost Effective SRM Drive using Commercial 6-Switch IGBT Modules. In Proceedings of the 37th IEEE Power Electronics Specialists Conference, Jeju, Republic of Korea, 18–22 June 2006.
20. Gairola, S.; Priti; Paliwal, L.N. New Power Converter for SRM Drive. In Proceedings of the 2010 International Conference on Power, Control and Embedded Systems, Allahabad, India, 29 November–1 December 2010. [CrossRef]
21. Guan, M.J.; Liu, C.; Wang, K. A novel low-cost and high-performance converter topology for six-phase SRM. In Proceedings of the IEEE Vehicle Power and Propulsion Conference (VPPC), Hangzhou, China, 17–20 October 2016.
22. Hua, Y.C.; Yu, D.S.; Yan, Z.; Hu, Y.H. A Power Line Communication Method for SRG with Modified C-Dump Power Converter. In Proceedings of the 15th IEEE Conference on Industrial Electronics and Applications (ICIEA), Kristiansand, Norway, 9–13 November 2020.
23. Pires, V.F.; Foito, D.; Pires, A.J.; Cordeiro, A.; Martins, J.F. An 8/6 SRM Drive with a Multilevel Converter Based on an NPC Structure and Designed to Provide Transistor Fault Tolerant Capability. In Proceedings of the 2022 IEEE 16th International Conference on Compatibility, Power Electronics, and Power Engineering (CPE-POWERENG), Birmingham, UK, 29 June–1 July 2022.
24. Borecki, J.; Orlik, B. Novel, multilevel converter topology for fault-tolerant operation of switched reluctance machines. In Proceedings of the 2017 11th IEEE International Conference on Compatibility, Power Electronics and Power Engineering (CPE-POWERENG), Cadiz, Spain, 4–6 April 2017; pp. 375–380.
25. Chaurasiya, S.K.; Bhattacharya, A.; Das, S. Reduced Switch Multilevel Converter for Grid Fed SRM Drive to Improve Magnetization and Demagnetization Characteristics of an SRM. *IEEE Trans. Ind. Appl.* **2023**, *59*, 6804–6816. [CrossRef]

26. Chaurasiya, S.K.; Bhattacharya, A.; Das, S. Reduced switch multilevel converter topology to improve magnetization and demagnetization characteristics of an SRM. In Proceedings of the IEEE International Conference on Power Electronics, Smart Grid, and Renewable Energy (PESGRE), Trivandrum, India, 2–5 January 2022.
27. Dong, L.; Liu, Y.; Ling, L.; Liao, X.; Wang, Z. Design of converter topology for switched reluctance wind power generator. In Proceedings of the International Conference on Materials Science, Energy Technology, Power Engineering, Busan, Republic of Korea, 25–27 August 2017.
28. Sun, Q.; Wu, J.; Gan, C.; Guo, J. Modular Full-Bridge Converter for Three-Phase Switched Reluctance Motors with Integrated Fault-Tolerance Capability. *IEEE Trans. Power Electron.* **2019**, *34*, 2622–2634. [CrossRef]
29. Pires, V.F.; Pires, A.J.; Cordeiro, A.; Foito, D.A. Review of the Power Converter Interfaces for Switched Reluctance Machines. *Energies* **2020**, *13*, 3490. [CrossRef]
30. Mukhopadhyay, J.; Choudhuri, S.; Sengupta, S. Drive strategies for switched reluctance motor A review. In Proceedings of the Michael Faraday IET International Summit, Kolkata, India, 12–13 September 2015; pp. 132–135.
31. Murthy, V.V.N.; Tulasriram, S.S.; Amarnath, J. A New Converter Topology for Switched Reluctance Drive with Reduced Active Switching Devices. *Int. J. Recent Technol. Eng.* **2014**, *3*, 18–23.
32. Kolluru, A.K.; Kumar, M.K. Closed-loop speed control of switched reluctance motor drive fed from novel converter with reduced number of switches. *Int. J. Power Electron. Drive Syst.* **2020**, *11*, 189–199. [CrossRef]
33. Chandrasekaran, T.; Muthu Vinayagam, M. Performance analysis of a new converter for switched reluctance motor drive with component sharing. *Int. J. Power Control Signal Comput.* **2014**, *6*, 90–96.
34. Madhavi, M.; Tawde, P.; Gaikwad, S. Simulation of Switched Reluctance Motor Drive using Asymmetric Bridge Converter. *Int. J. Eng. Res. Technol.* **2021**, *10*, 345–349.
35. Arul Raj, R.; Shinde, R.; Selvendiran, R.; Uthra, R. A Closed Loop Speed Control of a Switched Reluctance Motor with a New Converter Topology. *IOSR* **2016**, *11*, 19–28.
36. Toledo, S.; Caballero, D.; Maqueda, E.; Cáceres, J.J.; Rivera, M.; Gregor, R.; Wheeler, P. Predictive Control Applied to Matrix Converters: A Systematic Literature Review. *Energies* **2022**, *15*, 7801. [CrossRef]
37. Ahuja, K.R.; Kumar, P.; Agarwal, L. Modeling and simulation of three-phasematrix converter using MATLAB. *Int. J. Adv. Res. Sci. Eng.* **2013**, *2*, 220–229.
38. Thiyaharajan, D. Quality improvement in matrix converter using venturini algorithm. *Int. J. Comput. Eng. Sci. Res.* **2018**, *5*, 78–83.
39. Hamane, B.; Doumbia, M.L.; Chaoui, H.; Bouhamida, M.; Chériti, A.; Benghanem, M. PI and RST Control Design and Comparison for Matrix Converters Using Venturini Modulation Strategy. *J. Power Energy Eng.* **2015**, *3*, 36–54.
40. Karaca, H.; Akkaya, R. Control of Venturini Method Based Matrix Converter in Input Voltage Variations. In Proceedings of the International MultiConference of Engineers and Computer Scientists 2009 (IMECS 2009), Hongkong, China, 18–20 March 2009.
41. Tambakhe, S.R.; Keswani, R.A. Analysis and stimulation of the matrix converter fed induction motor. *Int. Res. J. Eng. Technol.* **2021**, *3*, 2918–2925.
42. Kong, Q.Y.; Rong, Y.; Li, Y.C.; Liu, S.H.; Wang, F.X.; Qi, W.D.; Luo, Z.K. Research on Performance of Switched Reluctance Motor Based on Different Motor Poles. *Electr. Drive* **2020**, *50*, 93–97.
43. Zhou, Y.; Yan, J.G.; Liu, C.; Liu, D.Q. Research on Fault-tolerant Performance of Dualchannel of Aviation Switched Reluctance Generator. *Acta Aeronaut. Astronaut. Sin.* **2007**, *28*, 1146–1152.

Disclaimer/Publisher's Note: The statements, opinions and data contained in all publications are solely those of the individual author(s) and contributor(s) and not of MDPI and/or the editor(s). MDPI and/or the editor(s) disclaim responsibility for any injury to people or property resulting from any ideas, methods, instructions or products referred to in the content.